Detailed interpretation of the 5*f*-6*d* absorption spectrum of U^{3+} in Cs_2NaYCl_6 and high pressure effects based on an *ab initio* simulation

Fernando Ruipérez
Departamento de Química, C-XIV, Universidad Autónoma de Madrid, 28049 Madrid, Spain

Zoila Barandiarán and Luis Seijo[a)]
Departamento de Química, C-XIV, Universidad Autónoma de Madrid, 28049 Madrid, Spain and Instituto Universitario de Ciencia de Materiales Nicolás Cabrera, Universidad Autónoma de Madrid, 28049 Madrid, Spain

(Received 18 July 2007; accepted 11 September 2007; published online 11 October 2007)

The $5f \rightarrow 6d(t_{2g})$ absorption spectrum of U^{3+}-doped Cs_2NaYCl_6 is simulated with a quantum chemical *ab initio* embedded-cluster approach applied to U^{3+} substitutional defects of O_h local symmetry. The first-principles results help to provide a detailed interpretation of the very rich experimental absorption spectrum of this material between 14 000 and 25 000 cm^{-1}. Also, the effects of high pressures up to 26 kbars on the absorption spectrum are predicted, the most relevant feature being a redshift of around 21 cm^{-1}/kbar, which is the fingerprint of a bond length shortening upon $5f \rightarrow 6d(t_{2g})$ excitation. © *2007 American Institute of Physics*. [DOI: 10.1063/1.2794040]

I. INTRODUCTION

Experimental and theoretical studies on the $5f^{N-1}6d^1$ manifolds of actinide ions in solids are an important part of the quest for basic knowledge on the electronic structure of actinide bearing molecules and materials. Also important is their study under extreme conditions.

In U^{3+}-doped Cs_2NaYCl_6, the U^{3+} ions substitute for Y^{3+} in a high symmetry octahedral site with sixfold coordination, which makes it ideal for detailed observations, calculations, and analyses of the $5f^26d^1$ manifold. The absorption spectrum of this material was recorded for the first time by Karbowiak *et al.*[1] from 4000 to 25 000 cm^{-1} at 4.2 K. Besides the $5f^3 \rightarrow 5f^3$ absorptions, which were analyzed in detail, a set of very complex intense bands starting at 14 000 cm^{-1} was attributed to $5f^3 \rightarrow 5f^26d^1$ excitations without further analysis.[1] Seijo and Barandiarán[2] reported the results of *ab initio* embedded-cluster calculations on the energies of the $5f^26d^1$ manifold, which provided a sound support of the previous interpretation as well as details of the energetic location of individual electronic states; also, the observed bands were attributed not to single absorptions but to absorptions created by multiple electronic origins. No absorption intensities nor band profiles were calculated in that work. The energy range of the experimental absorption spectrum was further extended in Ref. 3 and a simplified model of interactions was formulated, according to which a number of individual assignments were made. Later, the assignments of the experimental absorption spectrum were revised by Karbowiak[4] at the light of the previous *ab initio* calculations of energy levels[2] and on the basis of new empirical crystal field theory calculations of energies and intensities.

In this work, we present *ab initio* calculations of the absorption intensities and absorption band profiles which complete the theoretical study initiated in Ref. 2 and which serve to provide a detailed interpretation of the very rich $5f^3 \rightarrow 5f^26d^1$ experimental absorption spectrum of U^{3+}-doped Cs_2NaYCl_6 between 14 000 and 25 000 cm^{-1} based on nonempirical calculations. Although most of the assignments of the experimental $5f^26d^1$ manifold are confirmed, a few discrepancies are found on the location of some electronic origins. Also, we predict the effects of high pressures up to 26 kbars on the $5f \rightarrow 6d(t_{2g})$ absorption spectrum, the most relevant feature being a redshift of around 21 cm^{-1}/kbar.

II. METHOD AND DETAILS OF THE CALCULATIONS

Assuming that the absorption spectrum of U^{3+}-doped Cs_2NaYCl_6 between 4000 and 25 000 cm^{-1} is due to transitions between electronic states which are mainly localized on the U^{3+} impurity and its first coordination shell, we performed wave function based relativistic *ab initio* calculations on the $(UCl_6)^{3-}$ cluster, under the effect of an embedding potential of Cs_2NaYCl_6.

The methods used here for the electronic structure calculations are the same as in the previous study of the energy levels[2] and only a few details of the calculations regarding the basis set and the level of correlation have been changed, which have been found to give good results on the $5f^3$ manifold of the U^{3+} free ion.[5] We summarize in brief the details. We used the *ab initio* model potential (AIMP) embedding method[6] with the Cs_2NaYCl_6 embedding potential produced in Ref. 7; relativistic effective core potentials of AIMP type for U ([Xe,4*f*] core)[8,9] and for Cl ([Ne] core);[10] a $(14s10p12d9f3g)/[6s5p6d5f2g]$ valence Gaussian basis set for U (Ref. 9) and a $(7s7p1d)/[3s4p1d]$ one for Cl (Refs. 10–12); the state-average complete active space self-consistent-field[13–15] (SA-CASSCF) method for static correlation (with a $[5f,6d,7s]^3$ CAS), followed by the multistate complete active space second-order perturbation

[a)]Author to whom correspondence should be addressed. Electronic mail: luis.seijo@uam.es

theory[16–19] (MS-CASPT2) method for dynamic correlation (48 3*s*, 3*p* electrons of the Cl ligands and 21 5*d*, 6*s*, 6*p*, 5*f*, 6*d*, 7*s* electrons of U were correlated) with the spin-orbit free relativistic Hamiltonian in a first step of the calculations; the spin-free state shifted spin-orbit configuration interaction method with single excitation [sfss-SOCI(s)] (Ref. 20) with the spin-orbit relativistic Hamiltonian, in a second step of the calculations, for spin-orbit coupling effects together with the previous dynamic correlation (the CI space was the CAS plus all single excitations from the active MOs). In the sfss-SOCI(s) calculations, we also computed the electric dipole transition moments from the ground state $5f^3(^4I_{9/2})\ 1\Gamma_{8u}$. We performed the SA-CASSCF/MS-CASPT2 calculations with the program MOLCAS (Ref. 21) and the sfss-SOCI(s) calculations with the program EPCISO.[22]

Using the bond lengths, breathing mode vibrational frequencies, adiabatic transitions, and absorption transition moments computed in the latter sfss-SOCI(s) calculations, we simulated the absorption profiles with the semiclassical time-dependent approach of Heller,[23,24] according to which the intensity profile of an individual absorption (one electronic origin) reads

$$I(\omega) = C\omega \int_{-\infty}^{\infty} \exp(i\omega t)\langle \phi | \phi(t)\rangle dt, \tag{1}$$

where ω is the frequency of the absorbed radiation, ϕ is the initial wave packet or vibrational wave function on the ground state, and $\phi(t)$ is its propagation in the final electronic state energy surface, which results from the vibrational time-dependent Schrödinger equation

$$i\hbar \frac{\partial \phi(t)}{\partial t} = H\phi(t)\ (\phi(0) \equiv \phi). \tag{2}$$

A widening factor Γ is usually included in $\langle \phi | \phi(t)\rangle$. The full absorption intensity profile is calculated as the superposition of the profiles of the individual electronic origins, with weight factors having the same ratios as the oscillator strengths of the individual absorptions. We have used a harmonic approximation for the vibrational Hamiltonian and we have only taken into account the totally symmetric (a_{1g}) breathing vibrational mode, which is the only one responsible for the intensity profile at first order. All the simulations presented in the paper used a widening factor of $\Gamma = 10\ \mathrm{cm}^{-1}$.

III. RESULTS AND DISCUSSION

A. Zero pressure results

We show in Table I the data of the individual electronic origins. The slight improvements in the theoretical treatments with respect to the calculations of Ref. 2 did not change the basic features of the transition energies, bond lengths, and breathing mode vibrational frequencies of the $5f^26d^1$ manifold, neither the order of the electronic states nor their main character. All these data, together with the oscillator strengths, were used to calculate the simulated absorption spectrum which is shown in Fig. 1 between 17 000 and 27 000 cm^{-1}. The individual bands are shown in Figs. 2–5

The calculated absorption spectrum is made of five individual bands that correspond very well with the five bands identified by Karbowiak[4] as bands I-A, I-B, I-C, I-D, and I-E. The intensities of bands I-A and I-C, which are associated with the $^4K_{11/2}$ and $^4G_{5/2}$ levels of the U^{3+} free ions, are underestimated in the simulations. In any case, the five bands are well defined and they can be analyzed independently. Before we do it, we must have in mind that the accuracy of today's state-of-the-art *ab initio* calculations on the $5f$-$6d$ spectrum of a material like $Cs_2NaYCl_6:U^{3+}$ is not as high as to reach an agreement with the individual experimental lines of only a few tens of cm^{-1}. Empirical crystal field theory calculations are able to reach so high agreements because they are designed to do it: the parameters of the empirical approach, which can be many, are chosen so that the deviations are minimal. In first-principles calculations like this, however, the agreement, if it does exist, is just a consequence of the validity of the basic equations, the adequacy of the physical model, and the proper choice of technical conditions like basis sets or configuration spaces. Since the accuracy is limited, here we will correct the profiles of the individual bands in order to make them resemble more closely the experimental profiles, under the conditions that only the smallest possible number of corrections is done and that they are all reasonable, meaning that they remain within the accuracies of the methods which are known by experience. The underlying assumption is that, if a good agreement with an experimental profile is reached after a minimum number of reasonable corrections of the raw profile, the corrections are reliable.

In Fig. 2, we show the band I-A, which is a multiorigin band associated with the electronic origins 1–4 (levels $1\Gamma_{8g}$, $1\Gamma_{7g}$, $2\Gamma_{8g}$, and $1\Gamma_{6g}$). The experimental band (Fig. 6) is a set of five lines evenly separated with the maximum intensity in the second and third lines, which is a relatively simple structure for a band with four electronic origins. The raw simulation (dotted line; see also Table I) gives the basic structure of the band, which is due to the fact that most of the intensity is carried out by origins 1 and 3 and, at the same time, the first phonon line of origin 1 and the zero-phonon line of origin 3 almost coincide. Origins 2 and 4 have low intensity but, whereas the intensity of origin 4 is so low that it does not affect the band profile, origin 2 should leave its footprint in the profile according to the calculation. The facts that origin 2 does not show up in the experimental profile and that the most intense lines in the simulation (excluding the low intensity vibrational progression built on origin 2) are the second, first, third, and fourth lines instead of second, third, fourth, and first lines (Fig. 6) suggest that the location of origin 2 might be underestimated. If we correct it by 130 cm^{-1} and reduce in 50% the oscillator strength of origin 1, which are reasonable corrections, the result is the full line in Fig. 2. This profile compares rather well with the experimental one.

Band I-B is shown in Fig. 3. It is a multiorigin band associated with the electronic origins 5–9 (levels $2\Gamma_{6g}$, $3\Gamma_{8g}$, $4\Gamma_{8g}$, $2\Gamma_{7g}$, and $5\Gamma_{8g}$). As with band I-A, the relatively simple structure of the experimental band for a band made of five electronic origins, on the one hand, and the comparison

TABLE I. Lower levels of the $5f^2 6d(t_{2g})^1$ manifold of U^{3+} in Cs_2NaYCl_6: Calculated bond lengths (R_e, in Å), breathing mode vibrational frequencies ($\omega_{a_{1g}}$, in cm^{-1}), adiabatic transition energies (T_e, in cm^{-1}), and oscillator strengths (f) from the ground state $5f^3(^4I_{9/2})1\Gamma_{8u}$ (R_e=2.698 Å, $\omega_{a_{1g}}$=318 cm^{-1}). The experimental zero-phonon lines (ΔE_{00}, in cm^{-1}) and the labels I-A–I-E of the five absorption bands have been taken from Ref. 4; the assignments of zero-phonon lines proposed in this work are indicated.

							ΔE_{00}	
	Electronic origin	Level	R_e	$\omega_{a_{1g}}$	T_e	$f\times10^3$	(Ref. 4)	(This work)
		Levels of main character $5f^2(^3H_4)\times6d(t_{2g})^1\Gamma_{8g}$						
Band I-A	1	$1\,\Gamma_{8g}$	2.666	314	16 905	3.73	14 158	14 158
	2	$1\,\Gamma_{7g}$	2.666	317	17 090	0.82		
	3	$2\,\Gamma_{8g}$	2.666	315	17 241	1.80		
	4	$1\,\Gamma_{6g}$	2.667	317	17 299	0.22		
Band I-B	5	$2\,\Gamma_{6g}$	2.667	315	18 195	4.19	15 684	15 684
	6	$3\,\Gamma_{8g}$	2.666	314	18 284	12.56		
	7	$4\,\Gamma_{8g}$	2.666	315	18 714	15.58	16 524[a]	
	8	$2\,\Gamma_{7g}$	2.663	317	19 072	0.40		
	9	$5\,\Gamma_{8g}$	2.667	316	19 175	1.01		
Band I-C	10	$6\,\Gamma_{8g}$	2.665	316	19 928	5.47	17 597	17 597
	11	$3\,\Gamma_{7g}$	2.668	316	19 965	1.65		
	12	$3\,\Gamma_{6g}$	2.665	316	20 356	1.63	17 774	17 774
		Levels of main character $5f^2(^3H_4)\times6d(t_{2g})^1\Gamma_{7g}$						
Band I-E	13	$4\,\Gamma_{7g}$	2.664	318	21 450	0.01	18 566	
	14	$7\,\Gamma_{8g}$	2.665	314	21 732	1.44	19 250	18 566
	15	$4\,\Gamma_{6g}$	2.664	319	21 859	0.01	19 544[b]	
	16	$5\,\Gamma_{7g}$	2.664	316	22 116	1.70		
Band I-D	17	$8\,\Gamma_{8g}$	2.665	316	22 297	16.12	19 740	19 250
	19	$9\,\Gamma_{8g}$	2.665	316	22 401	8.37		
		Levels of main character $5f^2$(other than $^3H_4$)$\times6d(t_{2g})^1$						
	18	$5\,\Gamma_{6g}$	2.665	315	22 302	3.62		
	20	$10\,\Gamma_{8g}$	2.665	316	22 732	4.62		19 740
	21	$6\,\Gamma_{7g}$	2.667	316	22 940	7.17		
	22	$6\,\Gamma_{6g}$	2.666	316	22 981	0.25		
	23	$1\,\Gamma_{8g}$	2.665	315	23 309	7.23		
	24	$12\,\Gamma_{8g}$	2.665	316	23 337	1.39		
	25	$7\,\Gamma_{7g}$	2.665	314	23 425	0.48		
	26	$3\,\Gamma_{8g}$	2.667	315	23 796	0.74		
	27	$7\,\Gamma_{6g}$	2.668	315	23 917	0.30		

[a]This line is assigned here as the first phonon of $4\,\Gamma_{8g}$, instead as its zero-phonon line.
[b]This line is assigned here as the first phonon of $8\,\Gamma_{8g}$ (origin 17).

between the raw simulation (dotted line; see also Table I) and the experiment (Fig. 6), on the other hand, suggest that approximate coincidences exist between lines of the vibrational progressions of different origins. If the zero-phonon line of origin 6 is shifted about −90 cm^{-1} so that it would almost coincide with the zero-phonon line of origin 5, the large and almost equal intensities of the two first prominent peaks would be explained. If, in addition, the intensity of origin 7 is reduced 50% and it is shifted about 50 cm^{-1} in order to get much closer to the superposition of the second phonons of origins 5 and 6, the structure of the third peak of band I-B (at around 16 300 cm^{-1}) can be explained. If this is so, the experimental line at 16 524 cm^{-1} assigned by Karbowiak to the zero-phonon line of $4\Gamma_{8g}$ would rather be its first phonon. Two facts may question this interpretation: the zero-phonon line does not show up and the 16 524 cm^{-1} line is very sharp. However, the zero-phonon line would lie in the tail of the second peak, which is more intense, and its interaction with it could result in a shorter, wider, and much less visible zero-

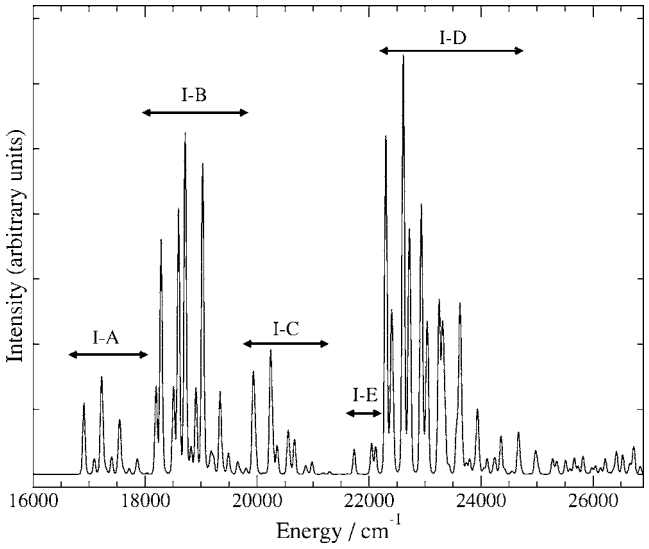

FIG. 1. Calculated $5f^3\rightarrow5f^26d^1$ absorption spectrum of $Cs_2NaYCl_6:U^{3+}$ up to 27 000 cm^{-1}.

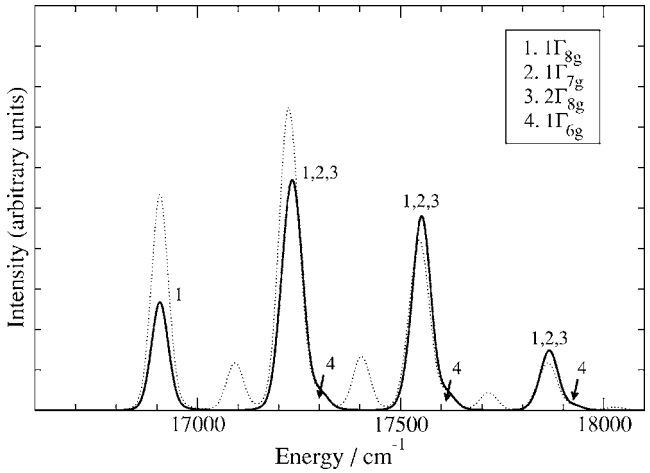

FIG. 2. Calculated raw (dotted line) and corrected (full line) intensity profiles of band I-A. The electronic origins 1–4 and their first respective breathing mode phonons are indicated.

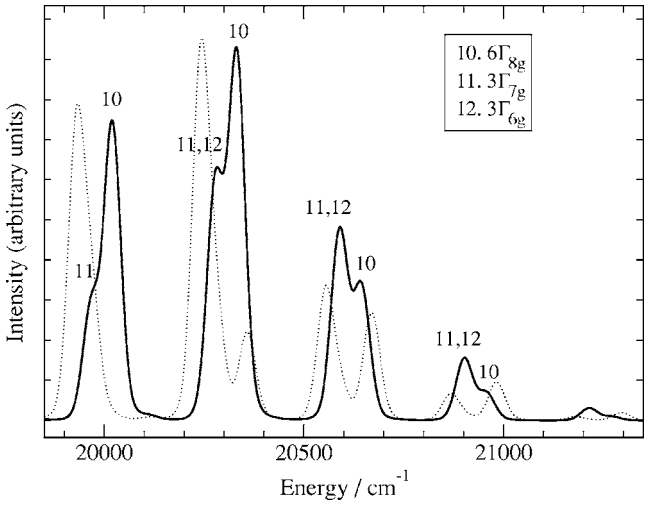

FIG. 4. Calculated raw (dotted line) and corrected (full line) intensity profiles of band I-C. The electronic origins 10–12 and their first respective breathing mode phonons are indicated.

phonon line. Regarding the second issue, although the sharpness of the 16 524 cm^{-1} line would indeed suggest a zero-phonon assignment, it is also compatible with a first-phonon assignment, as is shown by the equally sharp second peak of this band. On the other hand, the intensity profile of the fourth and fifth peaks supports the interpretation suggested by these calculations. In effect, the relative intensities of the fourth and fifth peaks do not resemble the relative intensities of the first and second peaks, which are built, respectively, on the zero phonons and first phonons of origins 5 and 6; however, they resemble very much the relative intensities of the fourth and fifth peaks, built on the first and second phonons. This interpretation cannot be taken as definite, however. The corrected simulated profile reproduces well the basic characteristics of the six evenly distributed peaks that constitute band I-B.

Band I-C is shown in Fig. 4. According to our calculations, it is a multiorigin band associated with the electronic origins 10–12 (levels $6\Gamma_{8g}$, $3\Gamma_{7g}$, and $3\Gamma_{6g}$). In the raw simulation (dotted line), origins 10 and 11 cannot be distinguished and the second, less intense peak that lies between the more intense first and third peaks of the experimental band does not show up. We shifted −90 cm^{-1} origin 12 and increased 50% its oscillator strength, as the only simple corrections that could reproduce the basic characteristics of the second peak. If origin 10 is shifted 80 cm^{-1}, the feature showing up on the left of the first prominent peak can also be reproduced. After these corrections, the simulated band profile reproduces rather well the basic features of the experimental band.

Band I-E is made of two small peaks just before the much more intense band I-D. These small peaks are very well reproduced in Fig. 5 and they correspond, respectively, to the zero-phonon line of origin 14 (level $7\Gamma_{8g}$) and to the superposition of its first phonon with the zero-phonon line of origin 16 (level $5\Gamma_{7g}$). Origins 13 (level $4\Gamma_{7g}$) and 15 (level $4\Gamma_{6g}$) are also in this area, but their intensity is very small to be detected; origin 13 is predicted to be around 300 cm^{-1} before origin 14 and origin 15 is next to origin 14. This interpretation differs from that of Ref. 4, where the peak at

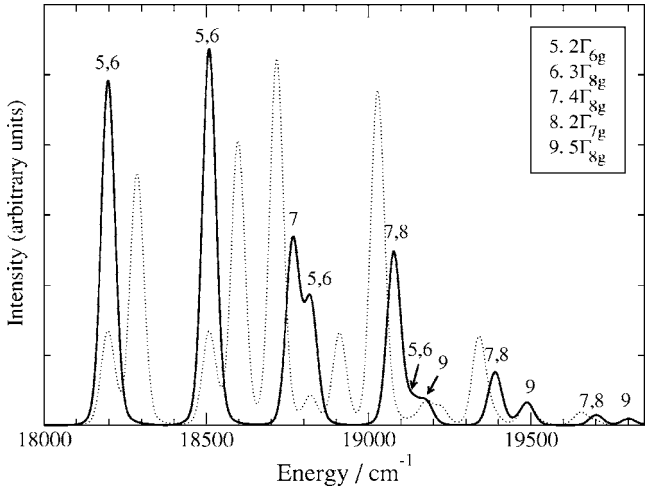

FIG. 3. Calculated raw (dotted line) and corrected (full line) intensity profiles of band I-B. The electronic origins 5–9 and their first respective breathing mode phonons are indicated.

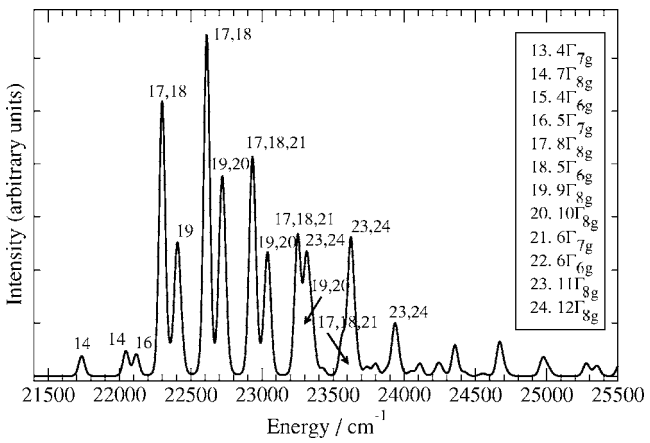

FIG. 5. Calculated raw (dotted line) and corrected (full line) intensity profiles of bands I-E (origins 14 and 16) and I-D (origin 17 and above). The electronic origins 14–24 and their first respective breathing mode phonons are indicated.

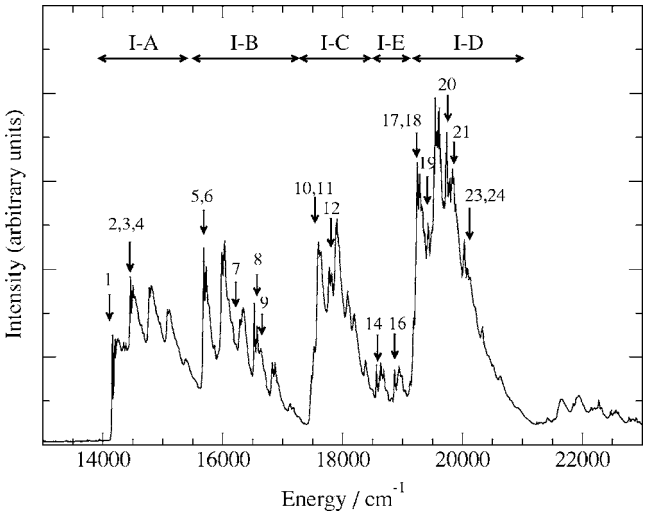

FIG. 6. Experimental absorption spectrum of $Cs_2NaYCl_6:U^{3+}$ at 4.2 K of Karbowiak *et al.* (Ref. 1) with arrows indicating the approximate location of the electronic origins suggested in this work.

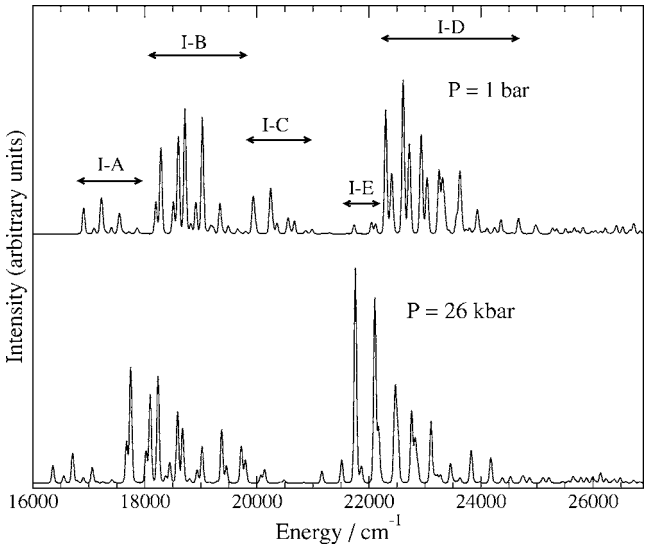

FIG. 7. Effect of high pressure on the calculated $5f^3 \rightarrow 5f^2 6d^1$ absorption spectrum of $Cs_2NaYCl_6:U^{3+}$ up to 27 000 cm^{-1}.

18 566 cm^{-1} was assigned to the zero-phonon line of $4\Gamma_{7g}$, the next peak to its first-phonon, and the levels $7\Gamma_{8g}$, $4\Gamma_{6g}$, and $5\Gamma_{7g}$ were located at higher energies, as part of band I-D.

The calculated profile of band I-D is shown in Fig. 5. This is a very complex band made of at least eight electronic origins (origin 17 and above) as indicated in the figure. The profile shows most of the basic characteristics of the experimental profile (Fig. 6) and the complexity of the band does not help to propose simple corrections that could improve the agreement, so that we did not do any corrections. Origins 17 and 18 (levels $8\Gamma_{8g}$ and $5\Gamma_{6g}$) are very close; their zero-phonon lines are responsible for the first peak, around 19 250 cm^{-1}, and their first phonon lines are responsible for the third peak, around 19 544 cm^{-1}. [The separation between these peaks, 294 cm^{-1}, is very close to the 302 and 300 cm^{-1} found in Ref. 3 for the breathing mode frequency of two different $5f^2 6d(t_{2g})^1$ states.] The assignment of these two peaks as the zero-phonon lines of $7\Gamma_{8g}$ and $4\Gamma_{6g}$ made in Ref. 4 does not fit our calculations; especially, the intensity of $4\Gamma_{6g}$ is too small to be observed. Regarding the second, less intense peak, our calculations suggest to assign it as the zero-phonon line of origin 19 (level $9\Gamma_{8g}$). Origins 20, 21, and 23 are intense and responsible for the characteristics of the second half of band I-D. In particular, the zero-phonon line of origin 20 overlaps the first phonon of origin 19 and gives a prominent line that corresponds very well with the experimental line at 19 740 cm^{-1}, which was previously assigned as the zero phonon of $8\Gamma_{8g}$.[3] Having in mind the limited estimated accuracy of the present calculations and not having had the opportunity of exploring reasonable empirical corrections for band I-D, we must consider the present assignments of the electronic origins responsible for band I-D less accurate than the others.

As a consequence of the previous analyses of the individual bands we propose the locations of the 24 first electronic origins of main character $5f^2 6d(t_{2g})^1$. They are shown in Fig. 6 together with the experimental spectrum.[1,4] This piece of information is a contribution based on first-principles grounds and it is independent of the empirical analyses that have been performed based on parametric crystal field theory calculations; both of them together help to draw a very detailed description of the very complex $5f^2 6d(t_{2g})^1$ experimental manifold of U^{3+} in Cs_2NaYCl_6 at zero pressure.

B. High pressure effects

We have calculated the energy curves of the ground state and the $5f^3 6d(t_{2g})^1$ states that correspond to the high pressures 13.2 and 26 kbars and, with them, the high pressure absorption profiles. In order to simulate hydrostatic pressure, we used representations of the Cs_2NaYCl_6 host with smaller unit cell constants than the zero pressure value $a = 10.7396$ Å (Ref. 25) ($a = 10.5463$ Å and $a = 10.3530$ Å, respectively), which correspond to relative volume shrinkages of $-\Delta V/V = 0.0530$ and 0.1042 and to the pressures mentioned above if the isothermal compressibility of the material is $\kappa = (-\Delta V/V)/P = 4 \times 10^{-3}$ $kbar^{-1}$.[26]

The absorption intensity profiles show a smooth variation with P. The one corresponding to 26 kbars is shown in Fig. 7. Bond lengths R_e, breathing mode vibrational frequencies $\omega_{a_{1g}}$, adiabatic transitions T_e, and zero-phonon transitions show a linear dependence on P in the studied interval, with all the states of main character $5f^2 6d(t_{2g})^1$ having almost identical slopes. As an example, the slopes for the level $1\Gamma_{8g}$ are $\partial R_e/\partial P = -0.001\,65$ Å/kbar, $\partial \omega_{a_{1g}}/\partial P = +1.4$ cm^{-1}/kbar, and a redshift of $\partial T_e/\partial P = -21.1$ cm^{-1}/kbar. The slopes of distances and frequencies of states of main configurations $5f^3$ and $5f^2 6d(e_g)^1$ are not significantly different; however, the slopes of the adiabatic transitions are very different and specific for the configuration. As examples, the absorption from the ground state $5f^3 - 1\Gamma_{8u}$ to $5f^3 - 1\Gamma_{7u}$ has an almost negligible shift of $\partial T_e/\partial P = -1.5$ cm^{-1}/kbar and the absorption to $5f^2 6d(e_g)^1 - 62\Gamma_{7g}$ has a very significant blueshift of $\partial T_e/\partial P = 66.6$ cm^{-1}/kbar. The redshift of the $5f^2 6d(t_{2g})^1$ states is the fingerprint of a bond length shortening upon $5f \rightarrow 6d(t_{2g})$

excitation and the blueshift of the $5f^26d(e_g)^1$ states the fingerprint of a bond length elongation upon $5f \rightarrow 6d(e_g)$ excitation, as discussed elsewhere.[27]

The profile at 26 kbars is shown in Fig. 7 together with the profile at zero pressure for comparison. The most significant effect of high pressure is a general redshift of 21 cm^{-1}/kbar. The spectrum keeps the structure of five different subbands with small modifications of the shapes. Only a couple of observations concerning origins 9 (level $5\Gamma_{8g}$) and 19 (level $9\Gamma_{8g}$) are worth mentioning. Origin 9 gains relative intensity [its oscillator strength changes from 1.91 at zero pressure to 5.55 at 26 kbars, whereas, for instance, origin 10 (level $6\Gamma_{8g}$) changes from 5.47 to 5.17], which rises the height of the end of band I-B with its zero-phonon and first phonon lines (calculated at 18 670 and 19 020 cm^{-1}) and makes less clear the limits between bands I-B and I-C. Origin 19 loses much of its intensity (from 8.4 to 0.04), which simplifies the structure of band I-D.

IV. CONCLUSIONS

We have simulated the absorption spectrum associated with $5f \rightarrow 6d(t_{2g})$ electronic transitions of U^{3+}-doped Cs_2NaYCl_6, out of the energy curves, and electric dipole transition moments produced in a relativistic, wave function based calculation on a $(UCl_6)^{3-}$ cluster embedded in an *ab initio* model potential representation of the Cs_2NaYCl_6 solid elpasolite. The first-principles simulation has provided a detailed interpretation of the very rich experimental absorption spectrum of the reference material between 14 000 and 25 000 cm^{-1}. Although the interpretation cannot be taken as definite, it complements previous experimental and crystal field theory based work and it confirms, corrects, and extends the knowledge of the $5f^26d(t_{2g})^1$ manifold of U^{3+} in Cs_2NaYCl_6. The effects of high pressures up to 26 kbars on the absorption spectrum have been predicted, the most relevant feature being a redshift of around 21 cm^{-1}/kbar, which is the fingerprint of a bond length shortening upon $5f \rightarrow 6d(t_{2g})$ excitation.

ACKNOWLEDGMENTS

The authors are very grateful to Professor M. Karbowiak and Professor J. Drożdżyński (University of Wroclaw, Poland) for the *X-Y* data of the absorption spectrum in Fig. 6. This work was partly supported by a grant from Ministerio de Educación y Ciencia, Spain (Dirección General de Investigación CTQ2005-08550).

[1] M. Karbowiak, J. Drożdżyński, S. Hubert, E. Simoni, and W. Strek, J. Chem. Phys. **108**, 10181 (1998).
[2] L. Seijo and Z. Barandiarán, J. Chem. Phys. **118**, 5335 (2003).
[3] M. Karbowiak and J. Drozdzynski, J. Phys. Chem. A **108**, 6397 (2004).
[4] M. Karbowiak, Chem. Phys. **314**, 189 (2005).
[5] F. Ruipérez, B. O. Roos, Z. Barandiarán, and L. Seijo, Chem. Phys. Lett. **434**, 1 (2007).
[6] Z. Barandiarán and L. Seijo, J. Chem. Phys. **89**, 5739 (1988).
[7] A. Al-Abdalla, Z. Barandiarán, L. Seijo, and R. Lindh, J. Chem. Phys. **108**, 2005 (1998).
[8] L. Seijo, Z. Barandiarán, and E. Harguindey, J. Chem. Phys. **114**, 118 (2001).
[9] L. Seijo, Z. Barandiarán, and B. Ordejón, Mol. Phys. **101**, 73 (2003).
[10] Z. Barandiarán and L. Seijo, Can. J. Chem. **70**, 409 (1992).
[11] T. H. Dunning and P. J. Hay, in *Modern Theoretical Chemistry*, edited by H. F. Schaefer III (Plenum, New York, 1977).
[12] S. Huzinaga, L. Seijo, Z. Barandiarán, and M. Klobukowski, J. Chem. Phys. **86**, 2132 (1987).
[13] B. O. Roos, P. R. Taylor, and P. E. M. Siegbahn, Chem. Phys. **48**, 157 (1980).
[14] P. E. M. Siegbahn, A. Heiberg, B. O. Roos, and B. Levy, Phys. Scr. **21**, 323 (1980).
[15] P. E. M. Siegbahn, A. Heiberg, J. Almlöf, and B. O. Roos, J. Chem. Phys. **74**, 2384 (1981).
[16] K. Andersson, P.-Å. Malmqvist, B. O. Roos, A. J. Sadlej, and K. Wolinski, J. Phys. Chem. **94**, 5483 (1990).
[17] K. Andersson, P.-Å. Malmqvist, and B. O. Roos, J. Chem. Phys. **96**, 1218 (1992).
[18] A. Zaitsevskii and J. P. Malrieu, Chem. Phys. Lett. **233**, 597 (1995).
[19] J. Finley, P.-Å. Malmqvist, B. O. Roos, and L. Serrano-Andrés, Chem. Phys. Lett. **288**, 299 (1998).
[20] R. Llusar, M. Casarrubios, Z. Barandiarán, and L. Seijo, J. Chem. Phys. **105**, 5321 (1996).
[21] G. Karlström, R. Lindh, P. A. Malmqvist, B. O. Roos, U. Ryde, V. Veryazov, P. O. Widmark, M. Cossi, B. Schimmelpfennig, P. Neogrady, and L. Seijo, Comput. Mater. Sci. **28**, 22 (2003).
[22] V. Vallet, L. Maron, C. Teichteil, and J.-P. Flament, J. Chem. Phys. **113**, 1391 (2000).
[23] E. J. Heller, J. Chem. Phys. **62**, 1544 (1975).
[24] E. J. Heller, Acc. Chem. Res. **14**, 368 (1981).
[25] C. Reber, H. U. Güdel, G. Meyer, T. Schleid, and C. A. Daul, Inorg. Chem. **28**, 3249 (1989).
[26] L. Seijo and Z. Barandiarán, J. Chem. Phys. **118**, 1921 (2003).
[27] F. Ruipérez, L. Seijo, and Z. Barandiarán, J. Chem. Phys. **122**, 234507 (2005).